Self-Assembly and Selected Area Growth of Zinc Oxide Nanorods on Any Surface Promoted by an Aluminum Precoat

Yee Wee Koh,[†] Ming Lin,[†] Chow Kim Tan,[†] Yong Lim Foo,[‡] and Kian Ping Loh*[,†]

Department of Chemistry, National University of Singapore, 3 Science Drive 3, Singapore 117543, and Institute of Material Research and Engineering, 1 Research Link, Singapore

Received: February 26, 2004; In Final Form: May 20, 2004

We demonstrate a simple method to direct the self-assembly of ZnO nanorods on flat and curved surfaces in hydrothermal synthesis by precoating the substrate with a thin film of aluminum (Al). The Al was transformed in the alkali hydrothermal environment into hydrotalcite-like zinc aluminum carbonate sheets, which provide a lattice-matched substrate for the self-assembly of ZnO nanorods. Selective growth of ZnO nanorods on the Al-patterned substrate as well as the high-density coating of carbon nanotubes by ZnO nanorods along the tangential and radial walls has been demonstrated using hydrothermal synthesis. The interfacial chemistry involved in the growth of ZnO and hydrotalcite-like zinc aluminum carbonate sheets is also discussed.

1. Introduction

The synthesis and controlled assembly of hierarchical array of nanorods in a two-dimensional fashion on a substrate are essential for device integration in photonic waveguides and directional lasing medium. Room temperature lasing action has been demonstrated from a highly oriented nanorod array of ZnO,[1,2] a direct band gap material with a large exciton binding energy of 60 meV. Highly ordered array of vertically oriented ZnO nanorods can be grown by vapor phase deposition methods on catalytically treated substrate[1,2] or on an epitaxial substrate such as sapphire.[3,4] In addition to the vapor phase deposition methods, the wet chemistry approach using hydrothermal synthesis has been shown recently to be a viable alternative to synthesize ZnO nanorods on a large-area wafer.[11] This method is economically attractive and industrially relevant as it allows industrial scale fabrication of large quantities of products at low cost. The chemistry aspects of ZnO growth in hydrothermal alkali environment have been reviewed previously by Demianets[5] as well as Vayssieres.[6−8] Vayssieres proposed that controlling the interfacial tension is the key to control the shape and the orientation of crystallites growing on a substrate from aqueous precursors. In aqueous system, crystal nucleation will be induced when the solution is supersaturated. Initial nucleation can occur either in solution (homogeneous) or on the surfaces of solid phases (heterogeneous), depending on the net interfacial energy of the system. If the interaction between the growing nucleus and a substrate surface represents a lower net interfacial energy, heterogeneous nucleation is favored over homogeneous nucleation. It is well-known that crystal−substrate adhesion energies (due to interfacial bond formation minus interfacial strain) can be dominant contributors to the net free energy for heterogeneous nucleation.[9] Thus far, almost all the templated hydrothermal synthesis methods rely on precoating the substrate with a ZnO buffer layer prior to the actual hydrothermal synthesis to promote high-density nucleation and oriented growth.[10−16] Because the ZnO buffer layer is prepared using chemical bath deposition, selected area synthesis via this approach is difficult. Moreover, regardless of whether vapor phase or wet chemical synthetic methods are used for the growth of ZnO, the growth is mostly demonstrated on flat, two-dimensional substrates.

In this work, we found for the first time that by precoating the substrate with a thin film of aluminum, the interfacial chemistry in an alkali hydrothermal environment readily promotes the growth of highly oriented ZnO nanorods on flat as well as curved substrates. We have also attained selected area hydrothermal synthesis of ZnO nanorods on aluminum-patterned substrate, attesting to the importance of interface control for nucleation in hydrothermal synthesis.

2. Experimental Section

Aluminum (Al) film was electron beam evaporated onto the different substrates used in these studies. These include silicon (100) wafer, carbon nanotube array, and polystyrene microbeads array fabricated on silicon. The thickness of Al film was varied from 5 mm to 1.2 μm to control the concentration of $Al(OH)_4^-$ in the hydrothermal synthesis. Zinc acetate was employed in the experiment as the Zn source, and the pH was adjusted to 10 using NH_4OH. The reaction was carried out in an autoclave at 100 °C for a reaction time of 2 and 9 h. The in-situ transmission electron microscope (TEM) experiment was performed with a JEOL 2010 system by mounting the sample on a carbon-coated copper grid and introducing onto a heating stage in the microscope. X-ray diffraction (XRD) measurements were performed using a Siemens Instrument operating with Cu Kα radiation (λ = 1.541 70 Å) at 40 kV/40 mA in the 2θ range from 5° to 70°. Scanning electron microscope (SEM) images were obtained using a JEOL JSM6700 microscope, operating at 10 A and 5 kV.

3. Results and Discussion

3.1. Oriented Assembly of ZnO on Flat Surfaces. The first series of experiments examined the conditions that can result in oriented assembly of ZnO nanorods on Al-coated surfaces. The strategy is to balance parameters like Al thickness on the substrate and Zn ion concentration. The objective is to identify the relative concentration of Al and Zn ions such that (1)

* Corresponding author. E-mail: chmlohkp@nus.edu.sg (K.P.L.). Fax: (65) 67791691.
[†] National University of Singapore.
[‡] Institute of Material Research and Engineering.

10.1021/jp049134f CCC: $27.50
Published on Web 07/02/2004

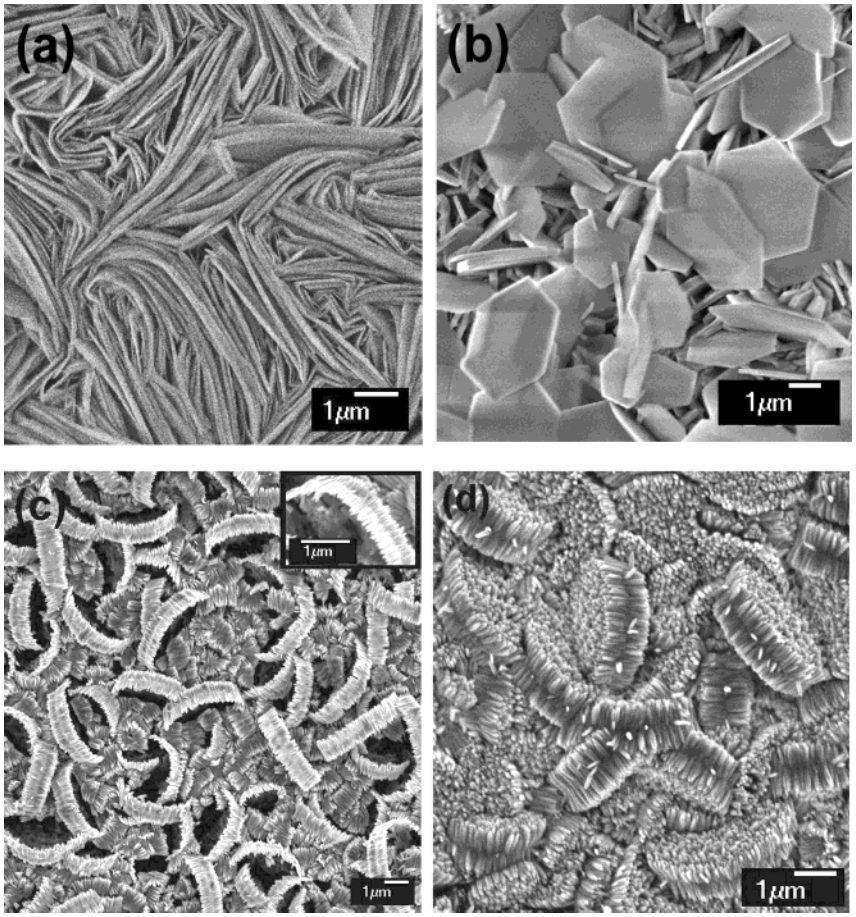

Figure 1. HTlc template grown at pH 10, 100 °C. (a) Thick multilayered HTlc sheets obtained when the Al thickness on silicon is ~1 μm in 0.31 M $Zn(Ac)_2$. (b) Isolated hexagonal HTlc plates obtained when Al thickness is ~1 μm in 0.016 M $Zn(Ac)_2$. (c, d) Various stages in the assembly of ZnO nanorods on HTlc template when Al thickness on silicon is ~100 nm in 0.016 M $Zn(Ac)_2$.

nucleation sites with low interfacial energies can be created on the substrate in a layered manner and (2) controlled heterogeneous nucleation proceeds *selectively* on these sites. It must be stated that for all the conditions we used here only sparsely populated, random ZnO nanorods could be grown on the bare substrate which was not pretreated with Al, and enhanced nucleation and oriented assembly arises only *after* precoating the substrate with Al films.

We discover that the Al film on the substrate is transformed in the alkali hydrothermal environment into aluminum carbonate hydroxide hydrate, which exhibits the morphology of hydrotalcite-like hexagonal sheets (here withal we will abbreviate the name of the compound as HTlc-$ZnAlCO_3$). By controlling the thickness of the Al film on silicon and the concentration of Zn^{2+} used in the hydrothermal synthesis, either thick multilayered HTlc sheets which roll up into a bundle (Figure 1a) or thin isolated hexagonal HTlc plates (Figure 1b) can be grown. Apparently the HTlc-$ZnAlCO_3$ acts as an excellent lattice-matched template for the assembly and growth of *c*-plane-oriented ZnO nanorods. Figure 1b−d displays the SEM images whereby we interrupted the hydrothermal synthesis at intervals to study the sequences in the assembly process, starting from the synthesis of the thin HTlC template initially, as shown in Figure 1b, to the oriented assembly of ZnO nanorods on the edges of the HTlc hexagonal template in Figure 1c, and finally to the complete oriented coverage of the HTlc template by ZnO nanorods in Figure 1d. The preferential nucleation on the edges of the HTlc template at first gives rise to belt-like ZnO nanorods array in Figure 1c; this might be related to the higher surface free energy on the faceted edges.

Figure 2a shows the images of ZnO nanorods which have self-assembled on the hexagonal HTLc template; the hexagonal shape of the template can be clearly observed by the manner in which all the ZnO nanorods packed to form two-dimensional hexagonal arrays. The changes in the crystal phases have been monitored by grazing angle XRD, as shown in Figure 2b. Initially, the diffraction peaks are due to the rhombohedral phase of HTlc-$ZnAlCO_3$ alone; after longer growth time, diffraction peaks due to hexagonal ZnO appear. From the SEM images, it is clear that the ZnO nanorods are oriented with their growth axis perpendicular to the hexagonal template and packed intimately. The ZnO nanorods are about 80 nm in diameter and have catalyst-free, pyramidal-shaped tips. High-resolution TEM images and diffraction pattern of the ZnO nanorod growing on the HTlc-$ZnAlCO_3$ are shown in parts a and b of Figure 3, respectively. The interplanar separation of 0.52 nm as indicated suggests that the growth axis is *c*-axis-oriented; thus, the (002) plane of the ZnO is oriented parallel to the (002) face of the rhombohedral HTlc template. The very tight packing density of the ZnO nanorods suggests a very efficient nucleation process on the HTlc template. Both faces of the HTlc template are available for nucleation. One individual, discrete unit of the ZnO array-on-HTLc platform in Figure 1d may act as a free-standing, micron-sized lasing array with hundreds of oriented ZnO nanorods or as a photonic waveguide unit.

If the silicon sample is coated with Al film of 5 nm thickness, the thinness of the Al layer allows the assembly of vertically aligned ZnO to proceed rapidly on the silicon substrate, possibly through an ultrathin HTlc-mediated interface that is oriented flat on the substrate face, and thus is not visible to SEM

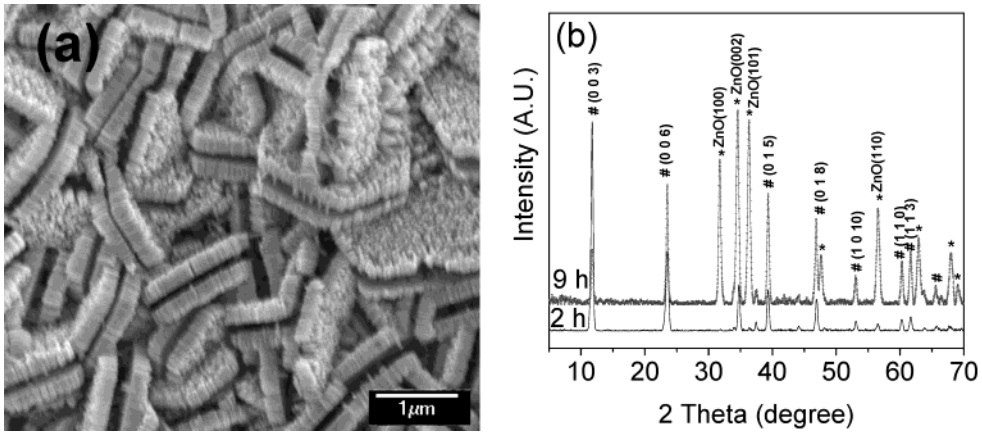

Figure 2. (a) SEM image showing the self-assembled hexagonal array of ZnO nanorods. (b) XRD pattern of ZnO nanorods grown on HTlc template, where the peaks can be assigned to HTlc-$ZnAlCO_3$ (#-labeled peaks) and ZnO (∗-labeled peaks). The presence of multiple diffraction peaks is due to the presence of differently oriented ZnO/HTlc platform, but within one ZnO/HTlc unit, the ZnO nanorods adopt only *c*-axis orientation on the HTlc.

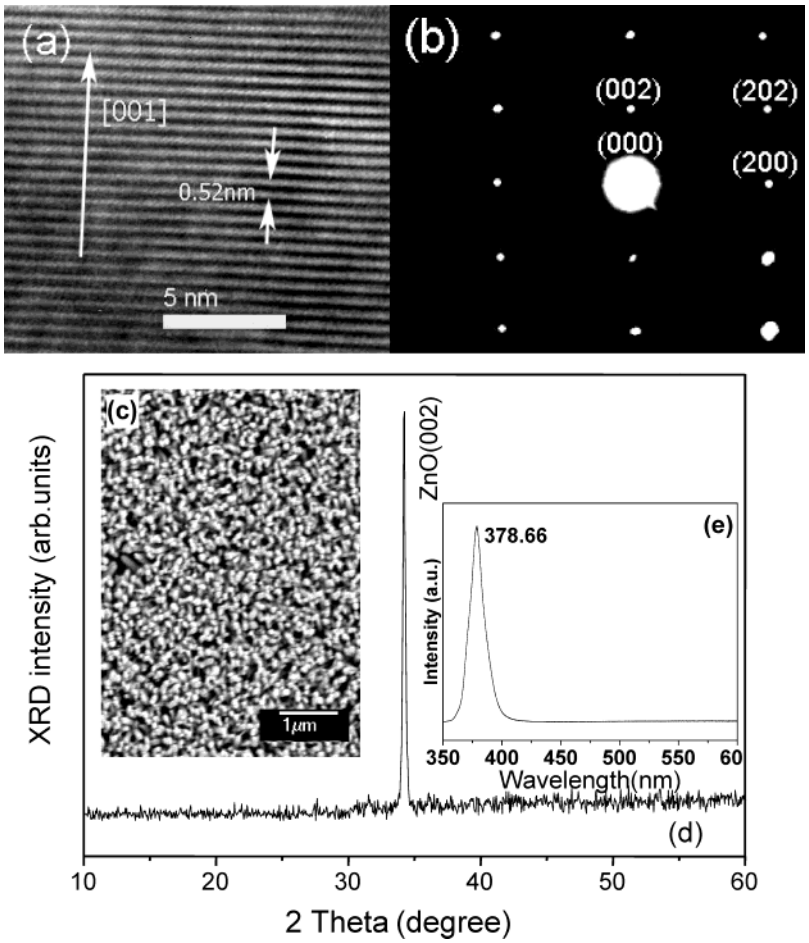

Figure 3. (a, b) HRTEM image and electron diffraction pattern of a ZnO nanorod, respectively. (c) Plane view SEM image of aligned ZnO nanorods synthesized on silicon coated with 5 nm Al film. (d) XRD 2θ scan showing only the (002) peak, indicating *c*-axis orientation. (e) Room temperature PL spectrum of aligned ZnO nanorods.

visualization. Oriented assembly of ZnO nanorods on the entire silicon sample face could be achieved via this approach, as shown in Figure 3c. Grazing angle XRD analysis of the ZnO-coated silicon sample shows only one strong (002) peak in Figure 3d, which is clear evidence of oriented assembly of the single crystalline ZnO nanorods with their (002) plane parallel to the silicon face. The control experiment which was carried out without the Al precoat obtained only sparsely distributed ZnO crystals that showed random orientation with respect to the plane of the silicon.

While we have demonstrated that Al-coated silicon is effective for the fabrication of oriented ZnO nanorods, one question is whether the presence of Al introduces deep trap centers in the energy gap of ZnO. Figure 3e shows the room temperature photoluminescence spectrum of the ZnO nanorods assembly, exhibiting only one single strong luminescence peak centered at 378.6 nm which is associated with the exciton recombination. The absence of defect-related or impurity-related trap centers indicates that the optical properties of ZnO nanorods fabricated this way are of excellent optical quality.

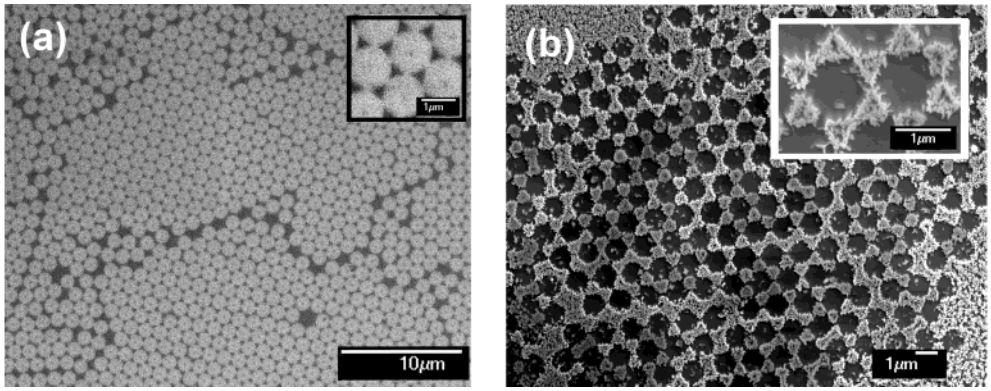

Figure 4. Selective growth of ZnO nanorods on patterned Al dots. (a) Patterned Al dots formed by the microsphere lithography method; the triangularly shaped black regions between the white circles are areas coated with Al. (b) Selective nucleation of ZnO on the Al-coated regions.

The heterogeneous growth suggests that the selective assembly of the ZnO nanorods should be possible by first lithographically patterning a thin film of Al on the substrate during hydrothermal synthesis. To demonstrate selective area growth on the Al-seeded areas, we apply the conventional microsphere lithography method to catalytically pattern the silicon surface with a hexagonal array of aluminum dots. Figure 4a,b demonstrates the patterned substrate before and after hydrothermal synthesis. Figure 4b shows that the formation of the ZnO nuclei is specific to the region coated with Al. This is very clear evidence that the hydrothermal conditions utilized in this work are operating in regimes where interfacial energy controls the nucleation.

3.2. Oriented Assembly of ZnO on Curved Surfaces. The challenge is to grow uniformly coated ZnO nanorods on curved surfaces. This is where hydrothermal synthesis affords unique advantages compared to vapor phase techniques due to the isotropic supply of reactants to the growing face in the solution phase. To evaluate this, carbon nanotube (CNT) array grown on silicon using chemical vapor deposition technique is used as the substrate. The CNT is precoated with ~5 nm thick Al film and then subjected to hydrothermal synthesis using similar growth conditions. Remarkably, both radial and tangential coating of the CNT with ZnO nanorods could be achieved, as shown in Figure 5a−c. The CNT two-dimensional array becomes a scaffold supporting high density of ZnO nanorods along the radial and tangential axis of individual nanotubes. The dimension of one single nanorod is about 30−50 nm, which is smaller that that obtained on the flat surface (~100 nm) shown earlier. This suggests that a curved surface will promote the growth of thinner ZnO rods due to the smaller contact area. Similar experiments have been carried out on Al-coated polystyrene microbeads that have been spin-coated on silicon using microsphere lithography. We find that uniform coating of the ZnO nanorods around the microbeads can be obtained as well, as shown in Figure 6a,b.

ZnO can have oxidative photocatalytical properties when it is excited with radiation with wavelength shorter than the energy of the band gap. During the photoexcitation process, holes and electron will be generated, and the holes can react with water and be converted into hydroxyl radicals which are strongly oxidizing species. These hydroxyl radicals can react with aromatic compound through diffusion-controlled process.[17] Our preliminary investigations show that supporting the ZnO nanorod on a 3-D scaffold enhances the effective surface area for photocatalysis compared to ZnO nanorod grown on 2-D substrate. In one experiment, both types of samples which had base silicon areas of 25 mm^2 were placed into beakers containing 5 mL of aqueous solution containing 30 ppm of phenol; these were then exposed to UV irradiation from a 125 W Hg lamp. After 5 h, no measurable change was detected from the sample containing ZnO nanorod grown on the flat silicon substrate, whereas a 10% reduction in phenol concentration could be detected from the sample containing ZnO-coated CNT array, suggesting that the higher density of 3-D supported ZnO nanorods is responsible for the improved photocatalytic effect.

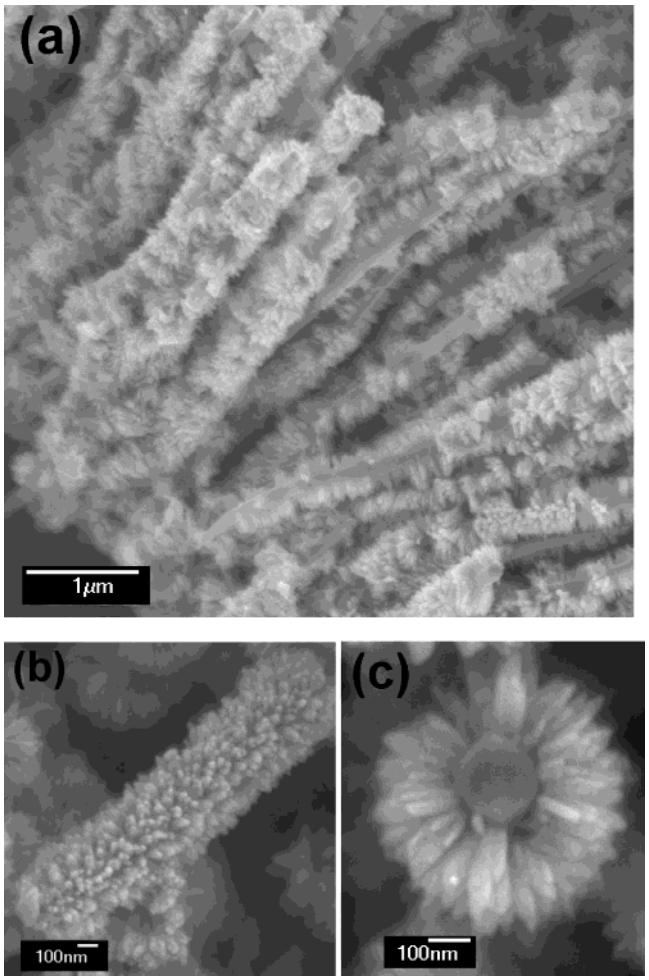

Figure 5. Three-dimensional assembly of ZnO nanorods on CNT: (a, b) side view of the ZnO−CNT system; (c) top view of the ZnO−CNT system.

TEM was applied to examine the stability of the interface between ZnO nanorod and CNT upon heating. The TEM images of the ZnO−CNT assembly are shown in Figure 7a,b. From Figure 7a, small hexagonal HTlc-like sheets are observed to adhere onto the CNT; we believe that these HTlc-like sheets

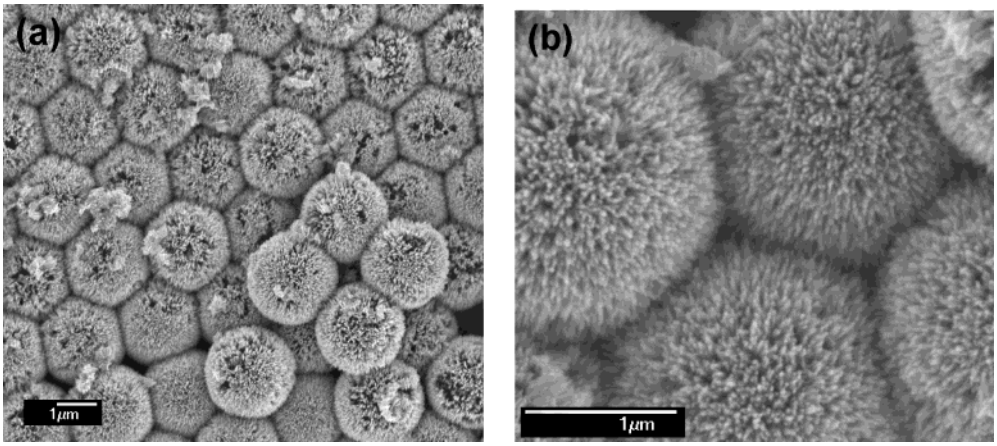

Figure 6. (a, b) Assembly of ZnO nanorods on Al-coated polystyrene spheres.

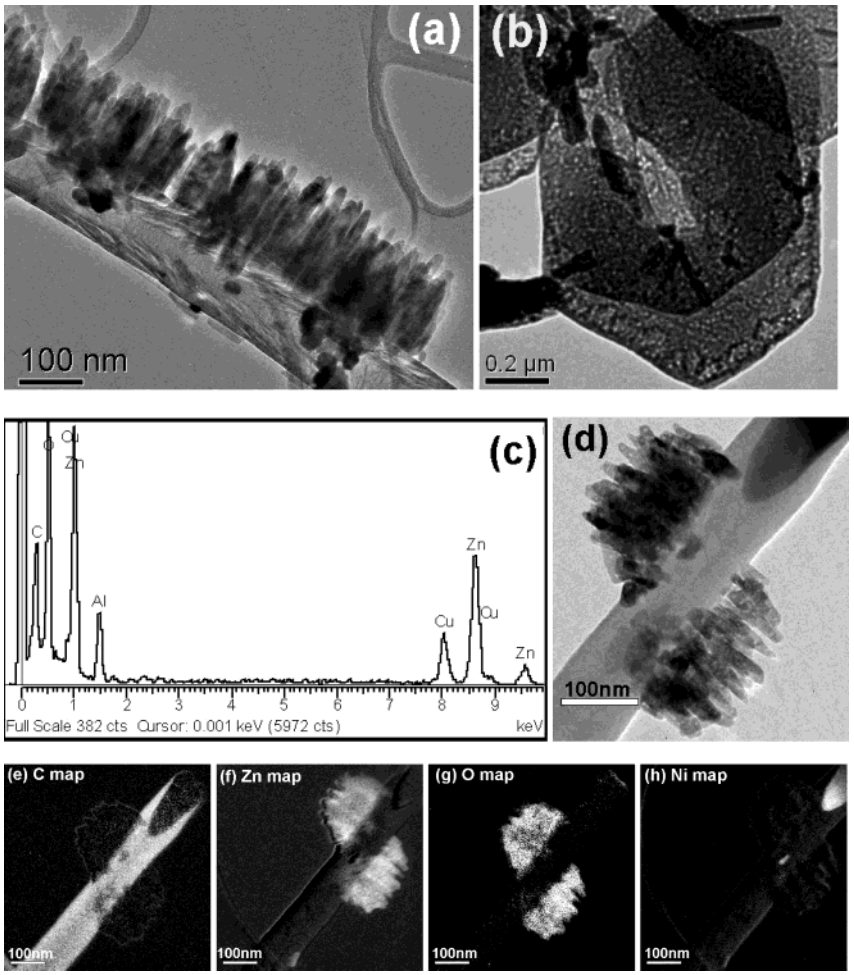

Figure 7. (a) TEM image of the ZnO−CNT system. (b) TEM image of hexagonal HTlc-$ZnAlCO_3$ sheet obtained when Al film is 100 nm thick. (c) EDX spectrum taken from the hexagonal HTlc-$ZnAlCO_3$ sheet shown in (b). (d) TEM image of ZnO−CNT before annealing. (e−h) EELS elemental mapping of ZnO−CNT shown in (d).

are responsible for the nucleation of ZnO on CNT. Energy dispersive X-ray (EDX) spectra recorded of a larger hexagonal sheet confirm the presence of Al and Zn. Elemental mapping of C, Zn, O, and Ni using electron energy loss spectroscopy (EELS) is shown in parts e−h of Figure 7, respectively. The presence of the element is evidenced by areas of bright contrast. The results, as anticipated, indicate that the nanorods consist of Zn and O. The element Ni is observed at the CNT tip because it is used as a catalyst for CNT growth. Figure 8 shows the images recorded in sequences of increasing heating temperatures. At the temperature when the Ni catalyst at the CNT tip starts to melt (>500 °C), we observed that the ZnO nanorods as well as the CNT−ZnO interface remains stable. No changes could be observed, except that the molten Ni is drawn into the CNT by capillary force. In fact, the interface between ZnO and CNT remains stable, i.e., no peeling off of the ZnO due to thermal shock occurs, until the evaporation temperature of ZnO in Figure 8c, where visible material loss from the ZnO nanorods can be seen.

3.3. Mechanism of Growth. The chemistry for the enhanced nucleation and ordered assembly of ZnO on Al-coated surfaces is interesting. The origin of the oriented growth observed here

is not intuitively obvious considering the lattice mismatch between Al and ZnO. Zn(II)-soluble species exist in the form of hydroxyl complexes such as $Zn(OH)_4^{2-}$ according to eq 1. In the current study, varying thickness of Al films between 5 and 1000 nm was deposited on the substrate. These Al films dissolve in the basic environment (pH > 9) as $Al(OH)_4^-$ according to eq 2. As shown in eq 3, the reaction between $Zn(OH)_4^{2-}$ and $Al(OH)_4^-$ will give rise to the formation of HTlc-$ZnAlCO_3$.

$$Zn^{2+} + OH^- \leftrightarrow Zn(OH)_4^{2-} \quad (1)$$

$$Al + OH^- \leftrightarrow Al(OH)_{4-} \quad (2)$$

$$(1-x)Zn(OH)_4^{2-} + xAl(OH)_4^- + (x/2)CO_3^{2-} + H_2O \leftrightarrow [Zn_{(1-x)}Al_x(OH)_2]^{x+}(x/2)CO_3^{2-}\cdot mH_2O + 2(1+x)OH^- \quad (3)$$

$$OH^-_{(surface)} + OH^-_{(soln)} \leftrightarrow O^{2-} + H_2O \quad (4)$$

$ZnAlCO_3$−HTLc belongs to anionic clays of general formula ($[M(II)_{1-x}M(III)_x(OH)_2]\cdot mH_2O$), a family of layered solids with positively charged layers (M(II) = Zn^{2+} or Mg^{2+}, M(III) = Al^{3+}) and interlayered charge-balancing anions.[18−20] The compound has been extensively studied as catalysts, anionic exchanges, and sorbents.[21,22] The divalent (Zn^{2+}) and trivalent (Al^{3+}) metal are localized in the same layer and occupy the octahedral holes in the close-packed configuration of the OH^- ions. The counteranions consist of carbonate ions and water which are freely migratable within the interlayer. Most of the synthetic HTlc are prepared by coprecipitation of the chosen M(II) and M(III) hydroxides with diluted NaOH or Na_2CO_3 solutions.[18−20] The calculated lattice mismatch between ZnO and HTlc-$Zn_{1-x}Al_xCO_3$ on the *a*-axis is about 5.78% if $x = 0.29$ (hexagonal ZnO, lattice constant $a = 3.2498$ Å, $Zn_{1-x}Al_xCO_3$ (hexagonal or rhombohedral), lattice constant $a = 3.052-3.079$ Å, depending on the ratio between Al and Zn).[23] The small lattice mismatch favors the nucleation of ZnO with its basal plane oriented parallel to the basal plane of HTlc-$ZnAlCO_3$. The preferential growth in the *c*-axis will give rise to well-aligned ZnO nanorods. In the actual experiments, controlling the concentration of Zn^{2+} and the thickness of the Al film is critical for allowing the correct sequences of reactions to proceed.

If the Al film is micron-sized thick, the high concentration of $Al(OH)_4^-$ allows homogeneous nucleation of HTlc-$ZnAlCO_3$ in solution, resulting in precipitation on the substrate in a random fashion. In this regime, we observe only the growth of HTlc-$ZnAlCO_3$ sheets without the formation of ZnO nanorods on it. The high concentration of $Al(OH)_4^-$ in this case consumes the $Zn(OH)_4^{2-}$ completely to form HTlc-$ZnAlCO_3$ and quenches the reaction for ZnO formation completely. This corresponds to the situation observed in Figure 1a,b where the Al film thickness was 1 μm. Reducing the Zn^{2+} ion concentration in (b) reduces the thickness of the HTlc-$ZnAlCO_3$ sheets such that isolated sheets could be obtained.

If the thickness of the Al film is reduced to 100 nm, the concentration of $Al(OH)_4^-$ is reduced by an order, and after complete reaction with $Zn(OH)_4^{2-}$ to form HTlc-$ZnAlCO_3$, the competing reaction to ZnO formation is quenched. The emergence of HTlc-$ZnAlCO_3$ surface at this stage allows the remaining $Zn(OH)_4^{2-}$ ions to nucleate and form ZnO nanorods. In this regime, heterogeneous nucleation responds sensitively to small changes in interfacial energies on the substrate. This is the case observed in Figure 1c,d, where we observe the sequential growth of oriented ZnO nanorod on the edges of the HTlc sheet at first, followed by the complete coverage of the HTLc sheet by the ZnO nanorods.

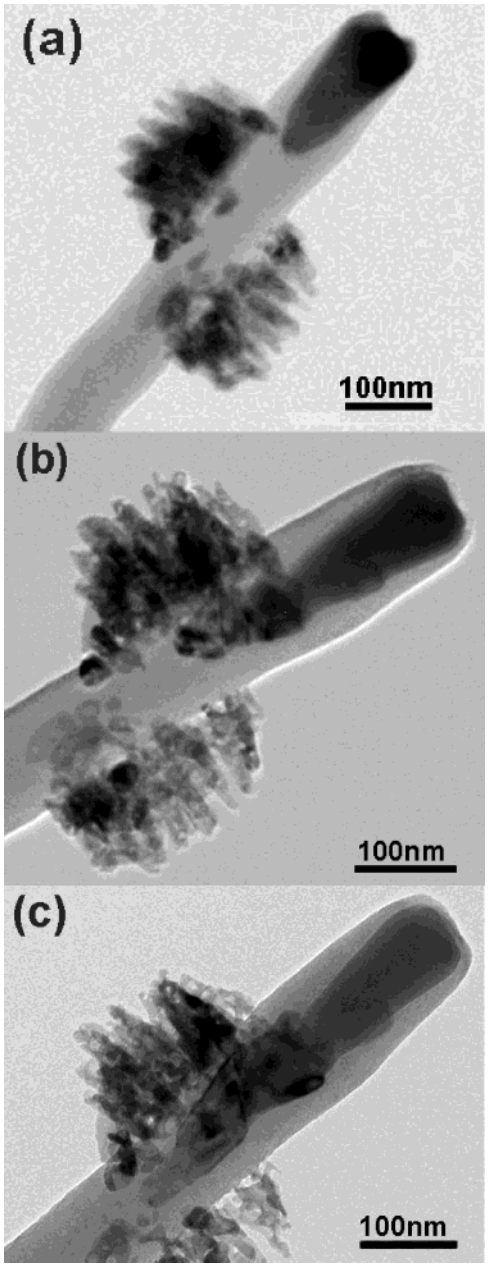

Figure 8. (a−c) TEM images of ZnO−CNT recorded in sequences of increasing heating temperatures. The interface remains stable until (c), where the ZnO nanorods start to evaporate in a vacuum; this occurs at temperatures >600 °C.

If the thickness of Al film is adjusted to less than 5 nm, the concentration of $Al(OH)_4^{2-}$ is about 2 orders smaller than the 100 nm thick Al. While most of the Al dissolves as $Al(OH)_4^{2-}$, a thin residual Al film might remain at the interface due to interfacial bonding between Si and Al. This Al layer can act as a seed layer for the heterogeneous nucleation of HTlc-$ZnAlCO_3$ with the basal plane arranged parallel to the substrate. The lattice mismatch between Al(111) and HTlc-$ZnAlCO_3$ for example is calculated to be ~5%.[23] Homogeneous nucleation is suppressed due to the much lower concentration of $Al(OH)_4^-$, and only an ultrathin layer of HTlc-$ZnAlCO_3$ nucleates by heterogeneous nucleation on the substrate. After the nucleation of the HTlc-$ZnAlCO_3$ layer with its basal plane oriented flat to the substrate face, the growth of the *c*-axis-oriented ZnO nanorods with vertical orientation to the substrate face proceeds, as shown in

Figure 3c. This is the most ideal stage for oriented assembly, and we find that very reproducible assembly of oriented ZnO nanorods can be achieved on a wide range of substrate if the thickness of Al film is maintained at ~5 nm on the substrates.

One clue to the excellent compatibility of the HTlc-$ZnAlCO_3$ sheet to act as a template for the nucleation of ZnO comes from examining the surface unit cell structure. The HTlc face is terminated by hydroxl groups, with a triangular unit cell of three OH surrounding a Zn (or Al) atom situated in the lower plane. The configuration of three OH around a central Zn on the OH-terminated face is very similar to the unit cell structure of ZnO with three O around the Zn on the oxygen-terminated face, with close lattice match between the two. At the initial stage of nucleation, the crystal structure of ZnO is gradually constructed by the dehydration between the OH^- on the surface of the HTlc and the OH^- of the Zn hydroxyl complexes according to the reaction shown in eq 4, driven by the high chemical potential of the OH^- in pH > 9 environment.

4. Conclusions

In conclusion, we have demonstrated a new and simple approach to fabricate ZnO nanorods in a vertically oriented fashion on both flat and curved surfaces by precoating the substrates with thin aluminum film of ~5 nm. The aluminum is transformed in the alkali hydrothermal environment to hydrotalcite-like zinc aluminum carbonate, which provides an excellent template for the assembly of ZnO due to epitaxial relationship with the (002) plane of ZnO. The synthetic strategies relied on controlling the concentration of the reactants to promote heterogeneous nucleation; the latter has been shown to respond sensitively to changes in interfacial energies. For example, we have demonstrated selective growth of ZnO nanorods on Al-patterned silicon substrate using hydrothermal synthesis. Most excitingly, the high-density and uniform growth of ZnO on curved surfaces such as carbon nanotubes array and polystyrene microbeads has been demonstrated to be possible using this novel method, suggesting a viable route to the large-scale assembly of oriented ZnO nanorods on any type of surfaces.

Acknowledgment. Professor Kian Ping Loh acknowledges the support of NUS academic grant R-143-000-221-112, FOS-NUSNNI, as well as Institute of Material Research and Engineering (IMRE) for support in this project.

References and Notes

(1) Huang, M. H.; Mao, S.; Feick, H.; Yan, H.; Wu, Y.; Kind, H.; Weber, E.; Russo, R.; Yang, P. *Science* **2001**, *292*, 1897.

(2) Govender, K.; Boyle, D. S.; O'Brien, P.; Binks, D.; West, D.; Coleman, D. *Adv. Mater.* **2002**, *14*, 1221.

(3) Park, W. I.; Kim, D. H.; Jung, S. W.; Yi, G. *Appl. Phys. Lett.* **2002**, *80*, 4232.

(4) Wu, J. J.; Liu, S. C. *J. Phys. Chem. B* **2002**, *106*, 9546.

(5) Demianets, L. N.; Kostomarov, D. V.; Kuz'mina, I. P.; Pushko, S. V. *Crystallogr. Rep.* **2002**, *47 (Suppl. 1)*, S86.

(6) Vayssieres, L. *Adv. Mater.* **2003**, *15*, 464−466.

(7) Vayssieres, L.; Keis, K.; Lindquist, S.; Hagfeldt, A. *J. Phys. Chem. B* **2001**, *105*, 3350.

(8) Vayssieres, L.; Keis, K.; Lindquist, S.; Hagfeldt, A. *Chem. Mater.* **2001**, *13*, 4395.

(9) Bunker, B. C.; Rieke, P. C.; Tarasevich, B. J.; Cambell, A. A.; Fryxell, G. E.; Graff, G. L.; Song, L.; Virden, J. W.; McVay, G. L. *Science* **1994**, *264*, 48.

(10) Tian, Z. R.; Voigt, J. A.; Liu, J.; Mckenzie, B.; Mcdermott, M. J. *J. Am. Chem. Soc.* **2002**, *124*, 12954.

(11) Greene, L. E.; Law, M.; Goldberger, J.; Kim, F.; Johnson, J. C.; Zhang, Y.; Saykally, R. J.; Yang, P. *Angew. Chem., Int. Ed.* **2003**, *42*, 3031.

(12) Boyle, D. S.; Govender, K.; O'Brien, P. *Chem. Commun.* **2002**, *1*, 80.

(13) Choy, J. H.; Jang, E. S.; Won, J. H.; Chung, J. H.; Jang, D. J.; Kim, Y. W. *Adv. Mater.* **2003**, *15*, 1911.

(14) Yamabi, S.; Imai, H. *J. Mater. Chem.* **2002**, *12*, 3773.

(15) Guo, M.; Diao, P.; Cai, S. M. *Acta Chim. Sin.* **2003**, *61*, 1165.

(16) Hung, C. H.; Whang, W. T. *Mater. Chem. Phys.* **2003**, *82*, 705.

(17) Sehili, T.; Boule, P.; Lemaire, J. *J. Photochem. Photobiol. A: Chem.* **1989**, *50*, 103.

(18) Allmann, R. *Chimia* **1970**, *24*, 99.

(19) Thevenot, F.; Szymanski, R.; Chaumette, P. *Clays Clay Miner.* **1989**, *37*, 396.

(20) Costantino, U.; Marmottini, F.; Nocchetti, M.; Vivani, R. *Eur. J. Inorg. Chem.* **1998**, 1439.

(21) Tichit, D.; Coq, B. *CATTECH* **2003**, *7*, 206.

(22) Cavani, F.; Trifiro, F.; Vaccari, A. *Catal. Today* **1991**, *11*, 173.

(23) Powder Diffraction Database JCPDS No. 481021-481024.